Ground-Based Remote Sensing of Cloud Particle Sizes during the 26 November 1991 FIRE II Cirrus Case: Comparisons with In Situ Data

S. Y. MATROSOV

Cooperative Institute for Research in Environmental Sciences, University of Colorado/NOAA/ETL, Boulder, Colorado

A. J. HEYMSFIELD

*National Center for Atmospheric Research, * Boulder, Colorado*

J. M. INTRIERI, B. W. ORR, AND J. B. SNIDER

NOAA/Environmental Technology Laboratory, Boulder, Colorado

(Manuscript received 4 April 1994, in final form 28 August 1994)

ABSTRACT

The paper presents the results of retrieving characteristic particle sizes for the November 26 1991 FIRE II case using two methods that utilize ground-based remote sensors. The size information for the complete vertical depth of the cloud was obtained for a 3-hour period from 1830 to 2130 UTC using combined Doppler radar and IR radiometer measurements and for two shorter periods using radar reflectivity and CO_2 lidar backscatter measurements. The results obtained with both remote sensing techniques are compared for these two periods. Possible retrieval uncertainties are discussed. Comparisons yielded an agreement with a relative standard deviation of 15%–20% between the two methods. Particle sizes retrieved by both methods were compared with 2D particle probe data sampled during 10 time intervals when a research aircraft was crossing the hub area. The relative standard deviation of particle sizes retrieved with the radar–radiometer method from those obtained from 2D probes is about 30% for nine compared times. The corresponding deviation for the lidar–radar method is about 35% for three compared times. The relative standard deviation between particle concentrations retrieved with the radar–radiometer method and those obtained from 2D probes is about 60% for nine compared times.

1. Introduction

Understanding the impact of cirrus clouds on the earth's radiation budget is very important for climate studies. Radiative properties of these clouds depend not only on their ice water amount but also on the characteristic sizes of ice particles (Takano et al. 1992). Ice particle sizes are responsible for the magnitude of the cloud shortwave albedo and hence for the modulation of the incoming solar radiation. The differences in the albedos of tropical and midlatitude cirrus clouds (the former generally have higher albedos) might be explained in part by particle size differences (Mitchell et al. 1994). For a given value of cloud ice water amount, an increase in particle characteristic size produces a decrease in shortwave reflectivity and longwave emissivity and an increase in shortwave transmittance (Ebert and Curry 1992).

Measurements of ice particle sizes from research aircraft are costly and most often limited to well-supported experiments. In addition, the volume of cloud sampled as well as the amount of data actually analyzed are usually small. This dictates a need for remote sensing techniques to measure parameters of ice clouds, which could eventually produce statistics about ice particle size occurrence under different meteorological conditions. Several recent studies were aimed at developing algorithms to infer ice particle sizes from satellite multichannel AVHRR (Advanced Very High Resolution Radiometer) passive measurements (Parol et al. 1991; Ou et al. 1994; Young et al. 1994). The retrieval in this case depends on the nonlinear relationships between radiances at various wavelengths. These nonlinear relationships vanish when characteristic particle sizes exceed a critical value. For ice particles this critical value is about 60 μm (expressed in effective radii) (Lin 1993).

Satellite measurements produce vertically averaged values of particle sizes, which in case of relatively dense clouds, are biased toward cloud tops. The ad-

* The National Center for Atmospheric Research is sponsored by the National Science Foundation.

Corresponding author address: Dr. S. Y. Matrosov, NOAA/ETL, R/E/ET6, 325 Broadway, Boulder, CO 80303-3328.

vantage of satellite measurements is the potential of obtaining global coverage; however, they need verification using microphysical data from aircraft in situ observations or data acquired by ground-based instruments. This study uses two techniques for estimating cirrus cloud microphysical parameters using combined ground-based measurements by different remote sensors. The description of instruments mentioned here and later are given in Intrieri et al. (1995). These techniques have been recently developed in the NOAA Environmental Technology Laboratory (ETL) and use the ETL remote sensors. They utilize the differences in the cirrus cloud signals as seen at different wavelengths.

An earlier version of the first technique (Matrosov et al. 1992) uses measurements of radar reflectivity and IR brightness temperature by a vertically pointed radar and a narrow field-of-view IR radiometer operating in the transparency "window" of 10–11.4 μm. Application of this initial version of the radar–radiometer technique allows estimation of ice cloud particle characteristic sizes, concentrations, and ice mass contents averaged through the vertical extent of the cloud. With the additional Doppler information providing vertical motion inside the cloud, the particle fall velocities are estimated, and vertical profiles of the cloud microphysical properties, mentioned above, are reconstructed. The modified method for retrieval of vertical profiles is described in detail by Matrosov et al. (1994) and is hereafter called RRT (radar–radiometer technique).

The RRT method is based on the difference in mechanisms responsible for radar backscatter and thermal IR emission of cirrus clouds. The radar signals depend mostly on scatterer volume for radar frequencies at the K_a-band and lower. However, the shape and density of scatterers are also important factors determining backscatter. The infrared brightness temperatures are determined by the cloud optical thickness (assuming that the temperature inside the cloud is known), which in turn is approximately proportional to the particle geometrical cross sections. K_a-band radar is inherently sensitive to larger particles, and radar pulses penetrate ice clouds almost without attenuation. The current sensitivity of the NOAA K_a-band radar does not allow sensing cirrus clouds with very small characteristic particle sizes (less than about 20–30 μm expressed in median diameters).

The second technique used in this study (Intrieri et al. 1993) utilizes measurements of vertical profiles of radar and CO_2 lidar ($\lambda \approx 10.6$ μm) backscatter to infer vertical profiles of cloud microphysical parameters. The particle size information in this technique is determined from the ratio of lidar and radar backscatter. Unlike radar signals, lidar signals are more sensitive to smaller particles but they suffer a substantial attenuation inside the ice clouds, and information about cloud optical thickness is needed to account for this attenuation. The optical thickness information is usually provided by the same type IR radiometer that is used in the RRT method. This technique is hereafter called LRRT (lidar–radar–radiometer technique). The LRRT method provides microphysical information from the cloud volumes from where both lidar and radar backscatter are measurable and attenuation of lidar signals is not complete.

During the First International Satellite Cloud Climatology Project Field Experiment FIRE-II experiment, NOAA's K_a-band radar, CO_2 lidar, and IR radiometer (modified Barnes PRT-5 narrowband radiometer) were located at the hub at Coffeyville, Kansas. One of the priority cirrus events of FIRE II was on 26 November 1991. This paper presents results for remotely sensed particle sizes for this event and compares the remotely sensed data with in situ measurements performed aboard the NCAR King Air aircraft.

2. Microphysical information from the radar–radiometer technique

a. Times of data gathering and IR measurements

On 26 November 1991, from approximately 1740 to roughly 2300 UTC, a persistent cirrus event was observed above the experiment site at Coffeyville. It should be mentioned that the lidar began seeing the cloud from about 1650 UTC. Neither the radar nor the IR radiometer detected the cloud until about 1740 UTC. During the first minutes after 1800 UTC the cloud was quite tenuous and produced a weak signal in the infrared. Several minutes prior to 1830 UTC the radar was performing scans and not looking vertically. Until about 1900 UTC the cloud was located primarily between 8 and 10 km above ground level. After 1900 UTC the cloud base descended rapidly to about 6 km and the cloud top descended more gradually to altitudes lower than 9 km. Figure 1 gives an illustration of the vertical extent of the cloud from 1830 to 2130 UTC. The gaps in this figure are due to nonvertical pointing of the radar and low-level clouds when the radar data were not used for the microphysical retrieval.

The minimum radar reflectivity value produced by the cloud and used for the further quantitative analysis was about −31 dBZ. The smaller values were not used because of the significant uncertainties of the radar calibration at such low levels of echo power. The data collected by the radar and IR radiometer after 1830 UTC were used for retrieval with the RRT method because after this time the measured reflectivities were consistently higher than −33 dBZ.

According to the data from the collocated and vertically pointed three channel microwave radiometer (90.0, 31.6, and 20.6 GHz), almost no liquid water was present inside the cloud until about 2130 UTC. Exceptions occurred during the period from 2000 to 2013 UTC when intervening low-level cloud patches were present and during occasional periods lasting only a

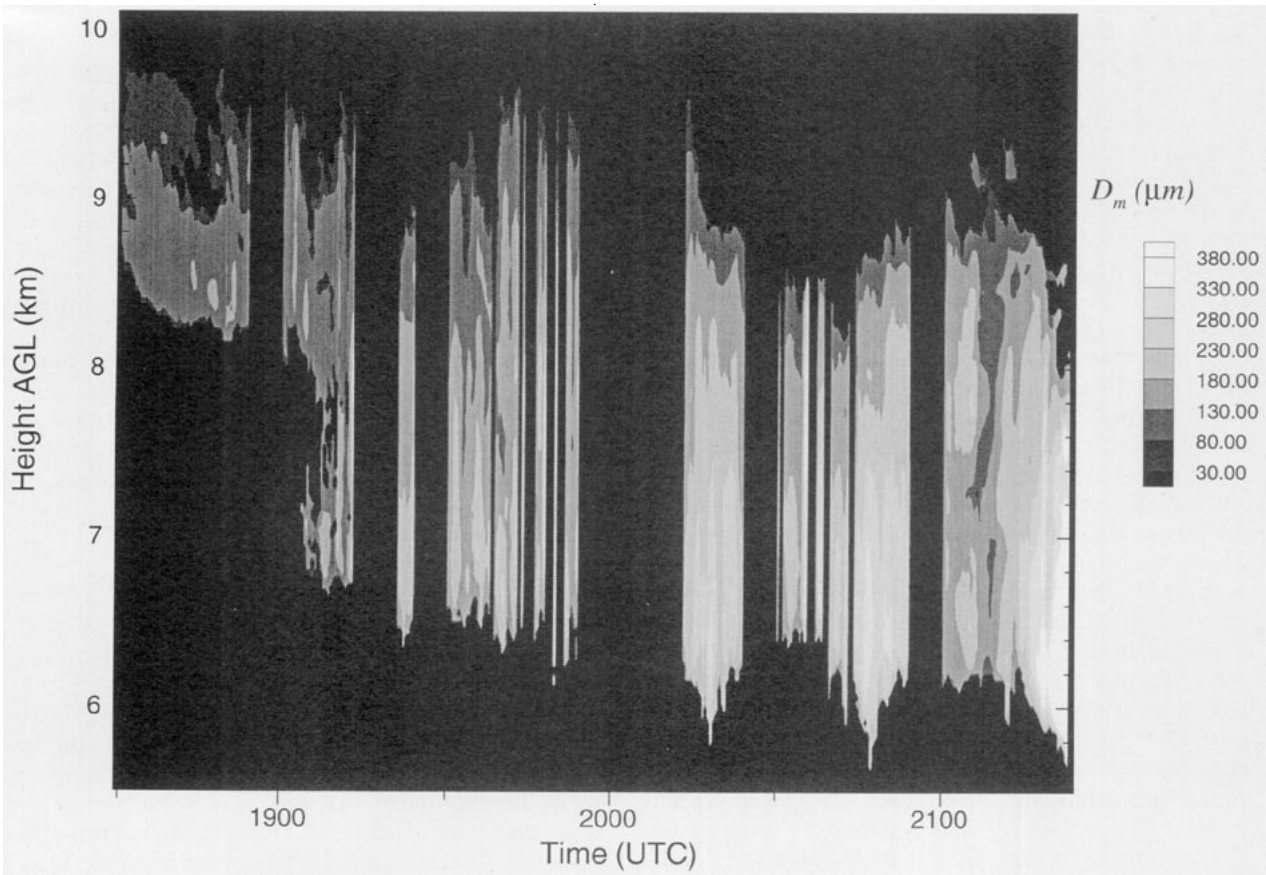

FIG. 1. Time–height cross section of retrieved particle size D_m during the FIRE-II cirrus event from 1830 to 2130 UTC 26 November 1991. Sizes are given for prolate-shaped particles with aspect ratio 2 in terms of median mass diameters of equal volume spheres for the first-order gamma distribution and density–size dependence (2). Retrieval was performed with the RRT method.

few minutes. After 2130 UTC the cloud thickened, and its base descended to altitudes below those usually associated with classic cirrus clouds. The microwave radiometer then began continuously showing the presence of liquid water.

The 3-h period from 1830 to 2130 UTC corresponded to a good realization of a predominantly ice cloud, which was easily detected by all the remote sensors. The maximum measured reflectivity during this period was about 4 dBZ. The data collected during this period were used to retrieve vertical profiles of cloud microphysical parameters. Time intervals with cloud liquid water present were not processed.

From approximately 1900 to 2100 UTC the CO_2 lidar signals were not able to penetrate to the upper boundary of the cloud because of the severe attenuation. However, during two time periods from 1834 to 1841 UTC and from 2113 to 2121 UTC when the cloud infrared extinction optical thickness (i.e., vertical integral of the extinction coefficient) τ_e was less than about 1.4–1.5, the lidar was performing vertical measurements, and its signals penetrated the full extent of the cloud. These two periods provided the opportunity to compare particle sizes retrieved by both RRT and LRRT methods in the entire cloud volume.

Calculations of the cloud extinction optical thickness were made in 30-s intervals for the entire 3-h period from ground-based measurements of IR brightness temperatures of downwelling radiation. Thirty-second intervals were dictated by the chosen IR radiometer integration time. In earlier versions of the RRT method (Matrosov et al. 1992, 1994) a two-stream radiative transfer model was used to determine the cloud absorption (τ_a) or extinction (τ_e) optical thickness. In this case a multistream discrete-ordinate model (Stamnes et al. 1988) with a changeable number of streams was used for this purpose. Infrared properties of nonspherical cirrus particles were modeled using the anomalous diffraction approximation (Chylek and Videen 1994).

As in earlier papers (Matrosov et al. 1992, 1994), measured brightness temperatures (T_{bm}) were recalculated into brightness temperatures at the cloud-base level (T_b) using the expression

$$B(T_{bm}) \approx B(T_b)P_a + B(T^*)(1 - P_a) + IP_a, \quad (1)$$

where T^* and I are the effective emitting atmospheric temperature and upwelling radiation reflected by the cloud and B and P_a are the Planck function and the atmospheric transmittance weighted by the radiometer spectral response. Note that in Matrosov et al. [1994, in Eq. (17)], which is similar to the above expression, the notation B for the Planck function was inadvertently omitted.

The parameters needed for estimation of τ_e and τ_a (i.e., cloud boundaries and the temperature and humidity profiles) were known from radar measurements and radiosonde data. The atmospheric transmittance P_a and optical depth of the atmosphere τ_{at} between the ground and the cloud were determined experimentally from IR brightness temperatures before the cloud developed (at about 1645 UTC) and theoretically using the Fast Atmospheric Signature Code (FASCODE) (Clough et al. 1988) calculations for the humidity and temperature profiles from the radiosonde launch at 1716 UTC. Both theoretical and experimental values for P_a and τ_{at} agreed very well. The corresponding value of P_a was about 0.91 for the radiosonde data. The value for P_a was adjusted continuously during the course of time, as the atmospheric water vapor amount was changing. This amount was monitored by the ETL three-channel microwave radiometer. Values of I were estimated according to Platt and Dilley (1979).

It should be mentioned that estimations of cloud absorption optical thickness τ_a from IR thermal measurements become a subject of substantial uncertainties for $\tau_a \geq 2.5$ because of the saturation effects. Note also that, for the IR window wavelengths (10–12 μm) and particle size distributions with characteristic sizes greater than about 40 μm, $\tau_e \approx 2\tau_a$.

A comparison of the radiosonde soundings at 1716 and 2025 UTC shows that temperatures at altitudes greater than 6 km changed very little (variations were usually within 1°C). This allowed the consideration of temperatures within the cloud to be mainly a function of height and not of time during the period of interest.

b. *Cirrus particle size from the radar–radiometer method*

Figure 1 shows the time–height cross section of the cirrus particle sizes retrieved using the RRT method. Radar reflectivity and velocity data were averaged in 30-sec intervals to match the averaging time of the IR radiometer. One vertical profile of particle sizes is shown for each such interval.

For 6 minutes at the end of each half-hour period the radar performed range–height indicator scans instead of looking vertically. These periods are shown as gaps in Fig. 1. Also shown as gaps are periods when the microwave and IR radiometers were indicating the presence of liquid water inside the cloud and a few 30-sec periods when retrieval of the cloud absorption optical thickness yielded $\tau_a \geq 2.5$.

The results of the retrievals shown in Fig. 1 are given in terms of the median mass diameters of equal volume spheres, D_m (hereafter called equivalent median diameters), but were obtained assuming prolate shape particles with aspect ratio $p = 2$. Such a choice was dictated by the analysis of two-dimensional particle probes from this cloud, taken from the King Air research aircraft. This analysis showed that the cloud contained mostly column-type particles and bullet-rosettes with aspect ratios of about 2. Such a particle shape is similar to one used by Minnis et al. (1993) for the midsize particle model.

When treating backscattering, the RRT retrieval scheme assumes spheroidal rather than hexagonal shape. This assumption is justified for radar applications because of recent findings (Dungey and Bohren 1993; Schneider and Stephens 1994) that show, for particles that are small compared to the wavelength, overall shape is important. However, slight differences in shape (like those of hexagonal particles, cylinders, and spheroids with the same aspect ratio) do not result in significant backscatter differences. In the infrared transparency window, where cirrus particles are optically "soft" and large compared to the wavelength, the anomalous diffraction theory is generally valid for extinction calculations. For the radar reflectivity calculations the spheroidal Rayleigh approach was used because it gives acceptable results even for the biggest cirrus particles of about 1.5 mm (Atlas et al. 1953; Matrosov 1993).

Direct microphysical studies show that the bulk density of cirrus particles decreases with an increase of their dimensions L as inferred from 2D particle images. Illingworth (1994) suggests that decrease to be proportional to $L^{-1.1}$. The effective bulk density for a 1-mm cirrus particle could be as low as about 0.05–0.1 g cm^{-3}, if the dimension L is taken as its spherical diameter (Heymsfield 1975). Summarizing this, the following empirical relationship is suggested for the cirrus particle bulk density ρ (in g cm^{-3}) as a function of particle 2D size, L, or equal volume sphere diameter, D, (in mm):

$$\rho = \frac{0.073(L/D)^3}{L^{1.1}} = \frac{0.073 r_L^{1.9}}{D^{1.1}}, \qquad (2)$$

where the coefficient r_L is the ratio of the particle 2D image size to its equal volume spherical diameter ($r_L = L/D$). The derivation of this coefficient for nonspherical particles is given in the appendix. The empirical equation for density (2) was used when performing the retrieval with the RRT method. For small particle sizes when (2) produces values greater than 0.916 g cm^{-3}, the solid ice density was assumed ($\rho_s = 0.916$ g cm^{-3}).

The retrieval was also made assuming that particle size spectra, in terms of the equal sphere diameters, are described by the gamma function of the first order:

$$N(D) = N_0 D^n \exp\{-(3.67 + n)D/D_0\}, \quad (3)$$

where D_0 is the median volume diameter and $n = 1$.

This function was shown to be appropriate (Kosarev and Mazin 1989) for describing experimentally measured cirrus particle size distributions. Two-dimensional probe measurements obtained from the aircraft in the cloud also showed that particle size distributions usually had exponential tails, which is consistent with the behavior of gamma functions at high values of argument.

For constant particle density the median volume diameter D_0 coincides with the median mass diameter D_m. For the density decrease with the increasing particle size, $D_m < D_0$. Two-dimensional particle size information is usually given in terms of median mass sizes, so for the convenience of comparisons of retrieved and in situ sizes the output of the RRT method was also given in terms of D_m. Figure 2 shows the ratio D_m/D_0 as a function of D_0 for the zero and first order gamma size distribution and several particle shapes. One can see that for the small particle sizes the difference between D_m and D_0 is negligible.

One of the input parameters in the RRT method is the exponent B in the particle size–fall speed (v_f) relationship. For an individual particle,

$$v_f = AD^B, \quad (4)$$

where D is the diameter of the equal volume sphere. The coefficient A is regarded as an unknown in this method because of its relatively high variability for natural ice crystals (Pruppacher and Klett 1978). Here A is determined for each 30-sec retrieval interval by matching the calculated value of cloud optical thickness with the value of τ_a determined from the IR brightness temperature measurements. The calculated value of τ_a is obtained from retrieved values of particle sizes and concentrations during an iterative procedure (Matrosov et al. 1994).

The values of the exponent B vary from about 0.7 to 1.4 for different natural ice crystals including snowflakes (Pruppacher and Klett 1978). In the tentative retrievals of cirrus particle parameters using the RRT method (Matrosov et al. 1994) it was assumed for simplicity that $B = 1$. Magono and Lee diagrams (1966) suggest, however, that ice crystals usually found at cirrus cloud temperatures of less than −20°C usually have values of B greater than 1 and values of $B < 1$ are, usually, typical for low-altitude planar snowflakes. The value of 1.1 was assumed when making the retrievals shown in Fig. 1.

The current version of the RRT method averages measured vertical Doppler velocities over long time periods (several hours) to cancel out most of the vertical air motion. This averaging is performed for small reflectivity intervals and as a function of height within a cloud. As a result, the fall velocity–reflectivity relationships are obtained for different radar range gates.

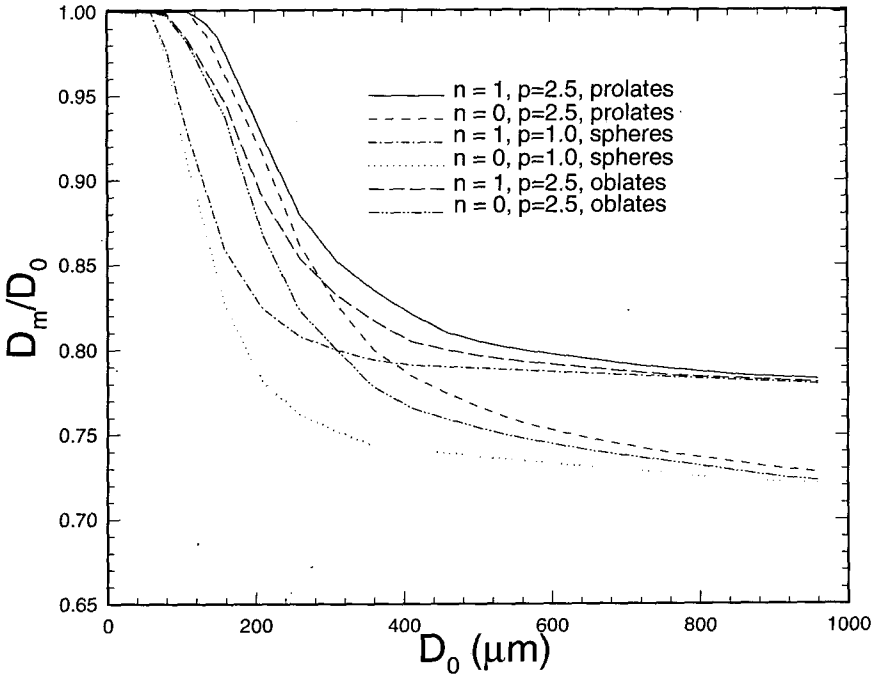

FIG. 2. The ratio of the particle median mass diameter to the median volume diameter as a function of the median volume diameter for the zero- and first-order gamma size distributions and several particle shapes.

These relationships are then used to estimate of vertical profiles of particle fall velocities in each 30-sec interval. Such averaging was performed for the entire interval of observations from 1830 to 2130 UTC.

Figure 3 shows the averaged vertical motion measured by a 404-MHz wind profiler for the same time period. One can see an obvious downward motion at cloud altitudes caused by descending cirrus particles. Examining altitudes below and above the cloud reveals, however, an average upward air motion of about 5–10 cm s^{-1}. The sensitivity of the retrieved results to the fall velocity bias is given in the next section.

One can see from Fig. 1 that equivalent median mass diameters D_m varied inside the cloud from about 35 μm to about 450 μm. The maximum sizes were observed near the cloud lower boundary. Particle sizes were generally increasing with time in the period from 1830 to 2130 UTC.

Figure 4 shows the scatterplot of radar reflectivities versus equivalent median diameters of particles. Reflectivity generally increases with an increase of characteristic particle sizes. The corresponding power law regression fit is

$$D_m = 334 Z_e^{0.23}, \tag{5}$$

where D_m is expressed in μm and Z_e in mm^6/m^3.

Possible variations in particle equivalent median diameters at reflectivity values of −38, −20, −10, and 0 dBZ are approximately 35–200, 75–280, 125–330, and 200–450 μm, respectively. The scatter in particle sizes diminishes as reflectivity increases. This significant scatter shows that there is no unique correspondence between particle sizes and reflectivity because Z_e depends not only on characteristic size of the particles but also on their concentrations.

The coefficients in the regression equation (5) were found for the dataset of 26 November 1991 and generally are not applicable to other datasets. These coefficients depend on meteorological conditions and would change from one observational situation to another. Because of these limitations of radar reflectivity data only, additional measurements are generally needed to get more accurate estimates of particle sizes. The RRT method uses estimates of particle fall velocities and cloud optical thickness for this purpose.

c. *Variation in particle sizes retrieved by the RRT method due to uncertainty in input parameters*

The particle size information presented above was obtained using the RRT method with basic set of a priori assumptions: the first-order ($n = 1$) size distribution of prolate particles with aspect ratio $p = 2$ and the bulk density–size relationship (2). The exponent B in the fall velocity–size relationship (4) was assumed to be 1.1.

Using different values of n, p, B, and a different density–size relationship as input information would alter the retrieved results. This also would change coefficients A_0 and B_0 in the regression relationship (4) [$A_0 = 334$ and $B_0 = 0.23$ in (5)]. To estimate the sensitivity of the retrieved particle characteristic sizes D_m to the a priori assumptions, a retrieval was performed with different a priori information. To assess this sensitivity quantitatively, the mean relative deviation (d_1), relative standard deviation (d_2), and the standard deviation (s) of two datasets (x_i and y_i) were calculated:

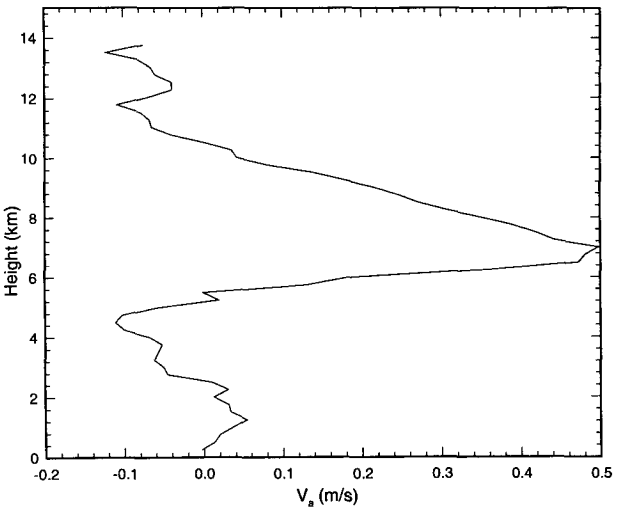

FIG. 3. Vertical profile of averaged vertical motion during the period 1830–2130 UTC obtained with 404-MHz wind profiler. Downward velocities are positive.

$$d_1 = \frac{1}{N}\sum_{i=1}^{N}\frac{2(y_i - x_i)}{x_i + y_i}, \tag{6}$$

$$d_2^2 = \frac{1}{N}\sum_{i=1}^{N}\frac{4(y_i - x_i)^2}{(x_i + y_i)^2}, \tag{7}$$

$$s^2 = \frac{1}{N}\sum_{i=1}^{N}(y_i - x_i)^2, \tag{8}$$

where N is the number of samples (about 14 000) for the considered time period. Note that d_1 reflects the general bias of one dataset relative to the other.

In Eqs. (6)–(8) x_i is the set of particle sizes, D_m, retrieved with the basic set of a priori assumptions mentioned above; y_i is the set of D_m retrieved when one of the assumptions is changed. Changing the assumed particle size distribution from the first ($n = 1$) to the zero ($n = 0$) order gamma function will result in $d_1 \approx -2\%$, $d_2 \approx 2.5\%$, and $s \approx 5$ μm. The coefficient A_0 in the best fit regression (4) will change just slightly (to 321 from 334), while the coefficient B_0 will change negligibly. Changes in the exponent B in the fall speed–size relationship (3) from 1.1 to 1.2 will cause $d_1 \approx 2\%$, $d_2 \approx 3\%$, $s \approx 4$ μm, $A_0 \approx 327$, and $B_0 \approx 0.22$.

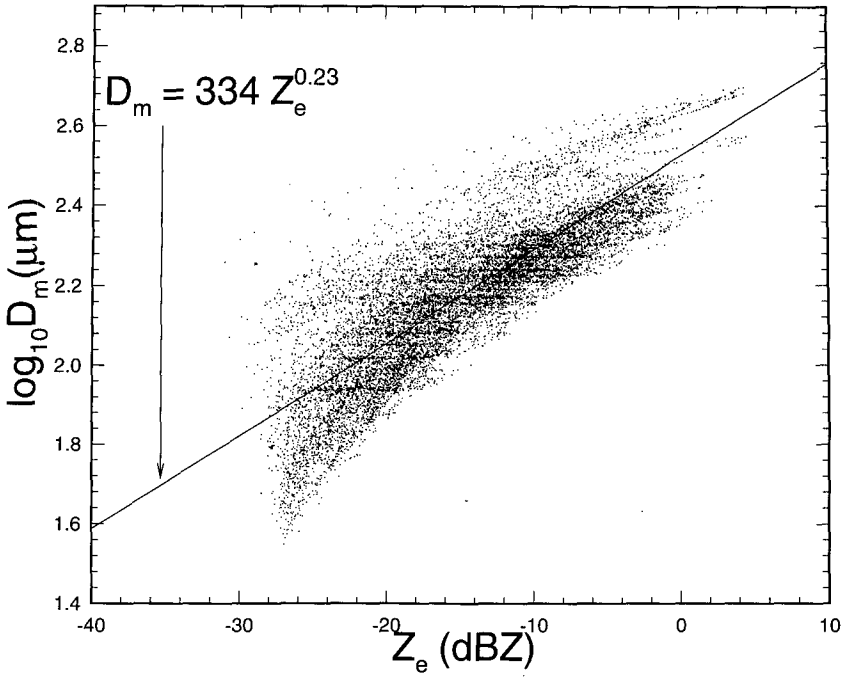

FIG. 4. Scatter plot of equivalent median mass diameter D_m (data were retrieved with the RRT method for 1830–2130 UTC November 26 1991) vs measured radar reflectivity for the same assumptions as in Fig. 1. Retrieval was performed with the RRT method.

To assess the sensitivity of the retrieved results to the cirrus particle density–size relationship, the value of the proportionality coefficient in (2) was changed by about 35% from 0.073 to 0.1. Such a change will yield $d_1 \approx -11\%$, $d_2 \approx 20\%$, $s \approx 35$ μm, $A_0 \approx 292$, and $B_0 \approx 0.23$.

If the particle density were constant, changes in the assumed particle shape from $p = 2$ to $p = 1$ (spheres) would result in only about a 4% change in the retrieved values of D_m. When density is size dependent, diminishing of density is different for particles with different shapes. This difference will be mostly due to changes in the coefficient r_L in (2), which depends on particle shapes (see the appendix). Such dependence will result in about a 20% increase in particle sizes when p changes from 2 to 1.

Some uncertainty still exists as to how well the mean air motion is removed when estimating particle fall speeds. As was mentioned before, a mean upward air motion of 5–10 cm s^{-1} was detected by the 404-MHz wind profiler during the period of observations (Fig. 3). In order to assess the sensitivity to the mean air motion, a retrieval was also performed with an increase of all particle fall speeds by 7 cm s^{-1}. Comparisons of the results in this case with those retrieved with undisturbed fall speeds yielded $d_1 \approx 4\%$, $d_2 \approx 9\%$, and $s \approx 11$ μm. The coefficients in the regression reflectivity–size relationship (5) for the case with the increase in fall speed are 310 (A_0) and 0.2 (B_0).

Such relatively small values of relative (d_1 and d_2) and absolute (s) deviations in this case are quite remarkable because they show that, for retrieval, the overall shape of the particle fall speed profile is more important than absolute values of fall speeds. It can be explained by the fact that the coefficient A in (4) is regarded as an a priori unknown and is found using real measurements of cloud optical thickness.

Finally, measurement error sensitivity analysis showed that uncertainty in measured values of Z_e of 1 dB would result in about 9% variations in retrieved particle sizes. A 10% uncertainty in the estimated value of cloud optical thickness would result in about 4% variations in D_m.

3. Comparison of particle sizes obtained with RRT and LRRT methods

As mentioned earlier, the comparisons of cirrus particle sizes retrieved with the RRT and LRRT methods for the entire depth of the cloud were available for only two periods from 1834 to 1841 UTC and from 2113 to 2122 UTC. This was due to a combination of factors including severe attenuation of lidar signals from approximately 1900 to 2100 UTC and performing (either by the lidar or by the radar) scans rather than looking vertically.

For the sake of comparison, LRRT-derived profiles of particle sizes were averaged in 30-sec intervals to

match the averaging time used by the RRT method. The particle sizes retrieved with the RRT method were also averaged over two consecutive radar range gates (37.5 m) to match the vertical resolution of the LRRT method dictated by the lidar vertical resolution (75 m).

The current version of the LRRT method treats cirrus particles as spheres with bulk density of 0.916 g cm^{-3}. To make the comparisons of this section meaningful, the RRT method was also run with the same assumptions. Note that for the case of constant density median volume diameters and median mass diameters are identical. It was also assumed in both methods that the particle size distribution is described by the gamma function of the first order.

It should be mentioned, however, that this set of assumptions in the RRT method produces values of D_m approximately 3% and 35% smaller (for the first and the second periods of comparison, respectively) than the basic set of assumptions for which the retrieval shown in Figs. 1 and 4 was made. The first comparison period produced smaller differences between basic and solid ice spheres assumptions than the second period because particle sizes were smaller during the first period (see Fig. 1) and, according to the relationship (2), their density was close to that of solid ice.

Figures 5 and 6 show the height–time cross sections of deviations of particle equivalent median diameter, D_m, values retrieved with the LRRT method from the values retrieved with the RRT method for the two periods of comparisons. These deviations were calculated using the expression under the summation sign in (6) for d_1. It can be seen that during the first period from 1834 to 1841 UTC the results of both methods agree quite well. For most of the volume inside the cloud deviations did not exceed ±15%. The relative and absolute standard deviations calculated using (7) and (8) yielded $d_2 \approx 15\%$ and $s \approx 15$ μm.

The comparison period from 2113 to 2122 UTC showed somewhat greater absolute deviations between the values of D_m obtained with the RRT and LRRT methods. Estimations of deviations produced $d_2 \approx 20\%$ and $s \approx 28$ μm.

For illustration, Figs. 7 and 8 show three individual vertical profiles of equivalent median diameters D_m retrieved with the RRT and LRRT methods for two 30-sec periods from both periods of comparison. Figure 7 depicts the profiles for the time period 1837:30–1838 UTC, and Fig. 8 the period 2118:30–2119 UTC. The estimated cloud extinction infrared optical thickness was about 1.3 during these second periods.

For the purpose of comparison two profiles of D_m are shown for the LRRT method. Curve 3 in Figs. 7 and 8 shows the results with accounting for attenuation of the lidar signals, which is the normal procedure. Curve 2 in these figures shows the results of the retrieval when this attenuation is neglected, illustrating the importance of the accounting for the attenuation. One can see that the RRT and LRRT methods agree much better in the upper part of the cloud when the attenuation is accounted for in the LRRT method. This accounting is especially important for clouds with substantial values of extinction optical thickness τ_e.

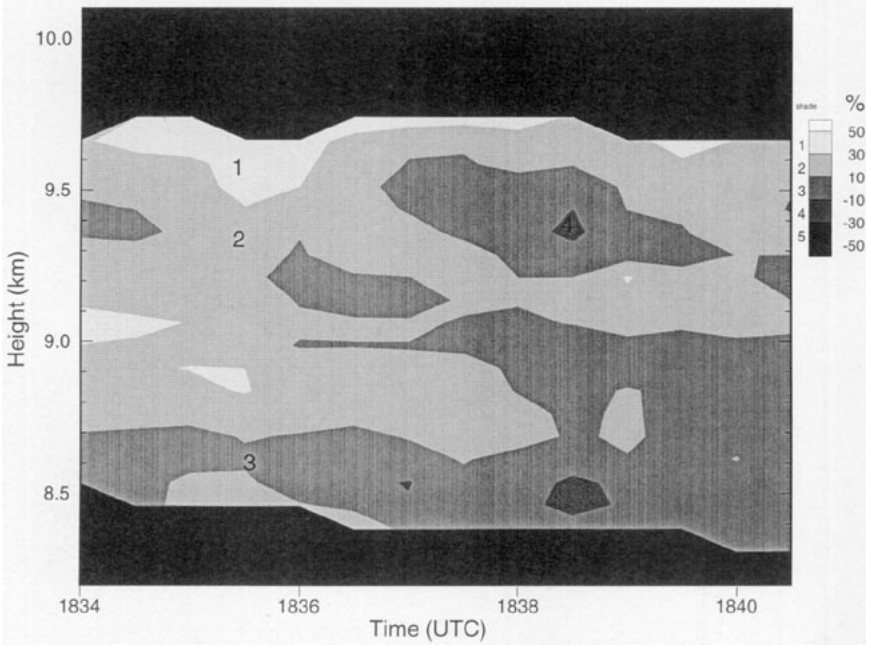

FIG. 5. Time–height cross sections of the deviation of median particle diameter D_m retrieved with the LRRT method from those retrieved with RRT method for 1834–1841 UTC November 26 1991. Deviations are given in percent.

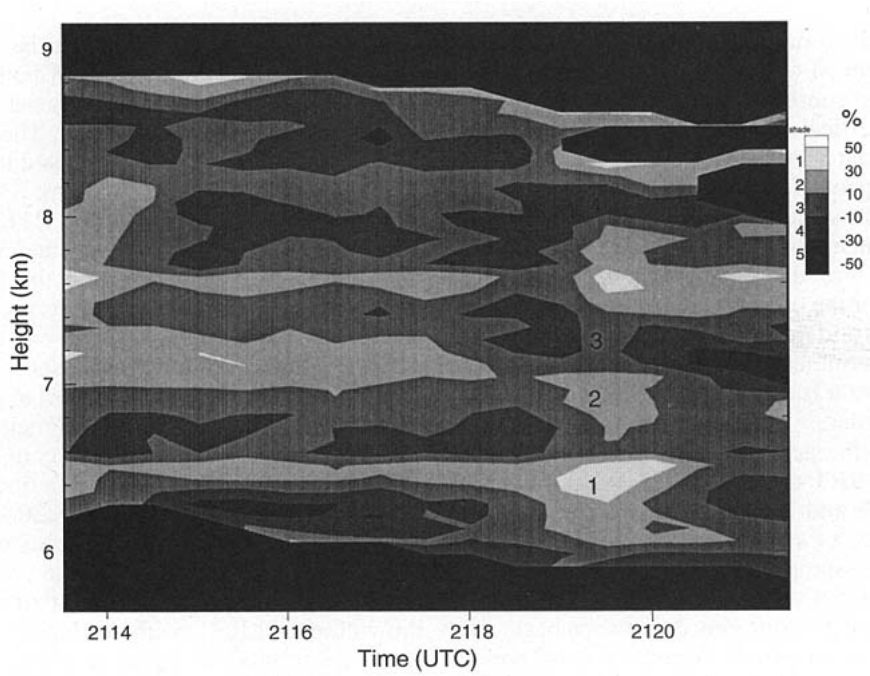

FIG. 6. As in Fig. 5 but for 2113–2122 UTC November 26 1991.

Summarizing the comparisons of the RRT and LRRT methods, we can state that they produce rather close results in terms of D_m and generally follow each other in the shape of the vertical profiles of particle sizes. Particle sizes generally increase toward cloud base.

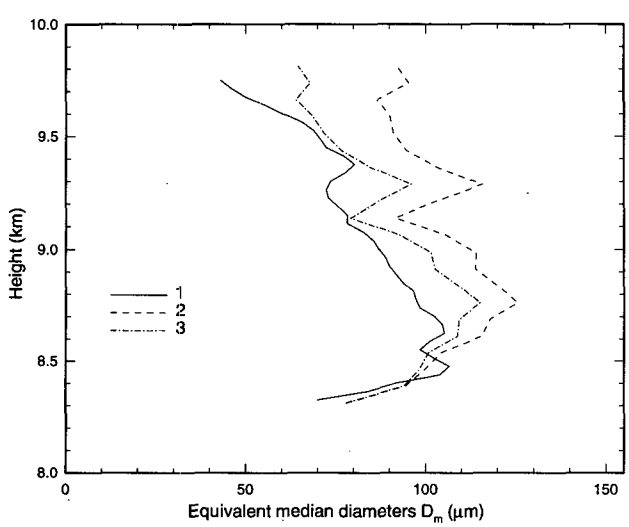

FIG. 7. Vertical profiles of particle equivalent median diameter D_m for the period 1837:30–1838 UTC retrieved with the RRT method (line 1), with the LRRT method without accounting for the attenuation of lidar signals (line 2), and with accounting for this attenuation (line 3).

4. Comparison of particles sizes retrieved from the ground-based and aircraft in situ measurements

The NCAR King Air research aircraft was flying a cirrus mission during the 3-hour period (1830–2130 UTC) being considered. The aircraft was equipped with two Particle Measuring Systems 2D probes to detect ice particles. The 2D-C probe sized particles from 25 μm to 1 mm in 25-μm increments. Particles smaller than 25 μm were partially accounted for in the smallest

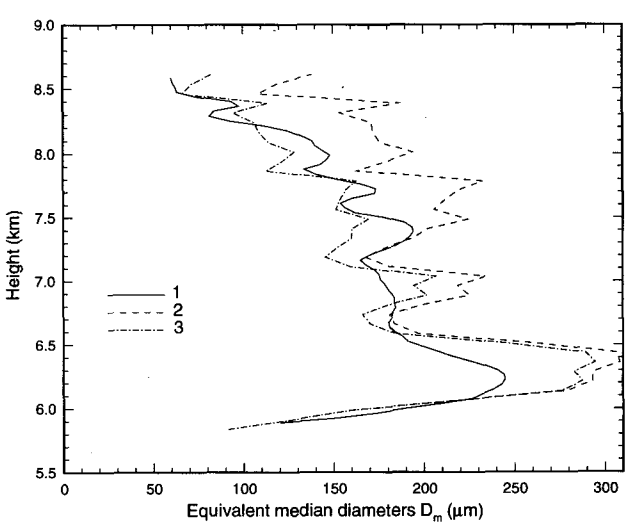

FIG. 8. As in Fig. 7 but for 2118:30–2119 UTC.

size bin. The 2D-P probe sampled particles from about 100 μm to 2 mm in 100-μm increments. The particle habits and size spectra were derived from composite 2D-C and 2D-P data. For each of the size spectra the particle concentration, ice mass content, radar reflectivity, and median particle size were derived as discussed by Heymsfield et al. (1990). Samples were taken at 5-s intervals.

Figure 9 shows a scatter plot of particle size versus radar reflectivity. Both parameters here were derived from the 2D probes. For the purpose of comparison the scale in Fig. 9 is the same as in Fig. 4 where retrieved particle sizes (with the RRT method) and measured radar reflectivities are shown. Note that in Fig. 9, as in Fig. 4, particle sizes are given in terms of median mass diameters of equal volume spheres, D_m, and were obtained by dividing major particle projection L, measured in 2D probes, by the coefficient r_L. The derivation of the coefficient r_L is given in the appendix. The best fit power law regression line for the aircraft data is

$$D_m = 330 Z_e^{0.184}. \quad (9)$$

It compares favorably with the regression fit from retrieved sizes and measured radar reflectivities (4).

Comparing Figs. 4 and 9, one can see that the aircraft data produce somewhat greater scatter with respect to the best fit line. In part, this can be explained by the fact that the aircraft and the ground-based instruments sampled different cloud volumes. Figure 10a shows the aircraft track during 3 hours of the comparison period. One can see that from 1830 until about 1930 UTC the aircraft was sampling clouds more than 100 km to the northwest from the hub at Coffeyville where the ground-based instruments were located. After 1930 UTC the aircraft returned to the vicinity of the hub.

Of direct interest are comparisons when the aircraft was sampling the cloud at the same (or nearly the same) volume as the ground-based sensors. Figure 10b shows the aircraft tracks when it was approximately above the hub. Also shown is the circle with a 3-km radius centered at the hub.

The aircraft made 15 passes through this circle. Four passes occurred during the 2000–2013 UTC time period when no remotely sensed data were collected because the cloud was obscured by the low-level liquid cloud patches. One pass happened to be when the radar was performing occasional RHI scans rather than looking vertically. Also, during one pass no microphysical samples were taken aboard the aircraft. This leaves nine passes for comparisons when both in situ (aircraft sampled) and remotely sensed data (from the RRT method) were available.

Decreasing the radius of the circle to less than 3 km would greatly reduce the number of potential points for comparison. Increasing this radius would lead to the possibility of comparing completely different cloud volumes. The times at which the chosen nine passes occurred were 1940, 1950, 2020, 2030,

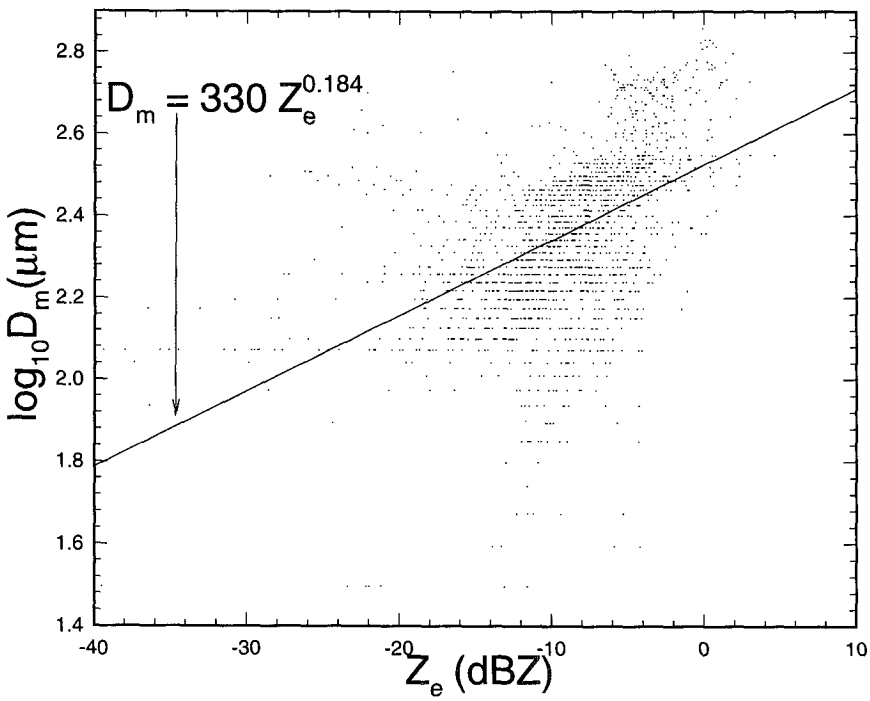

FIG. 9. Scatter plot of equivalent median diameter D_m vs radar reflectivity (aircraft data) for 1830–2130 UTC November 26 1991.

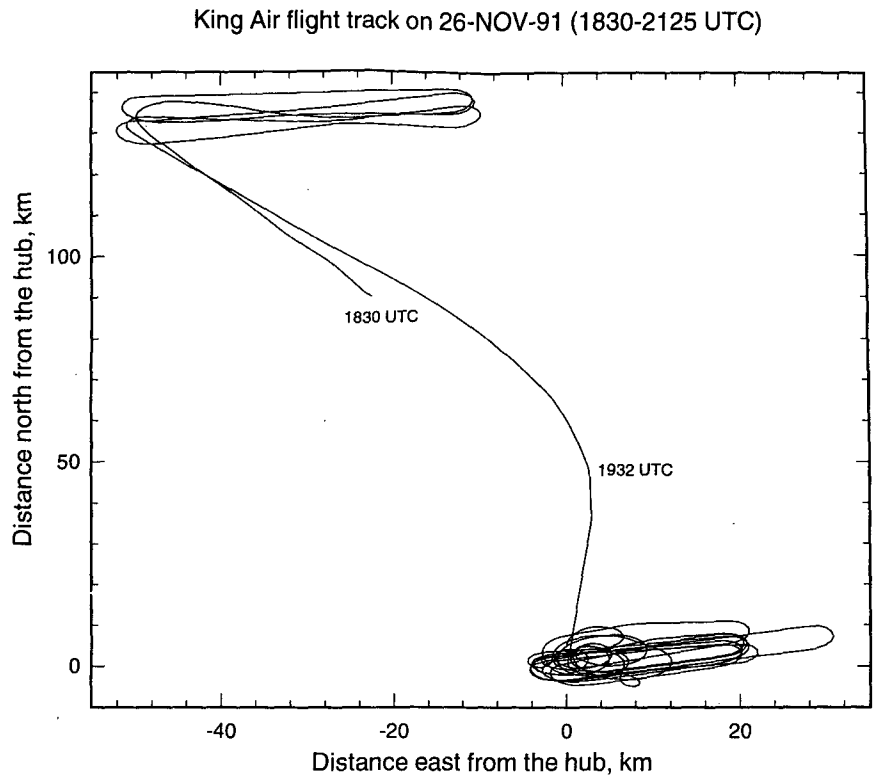

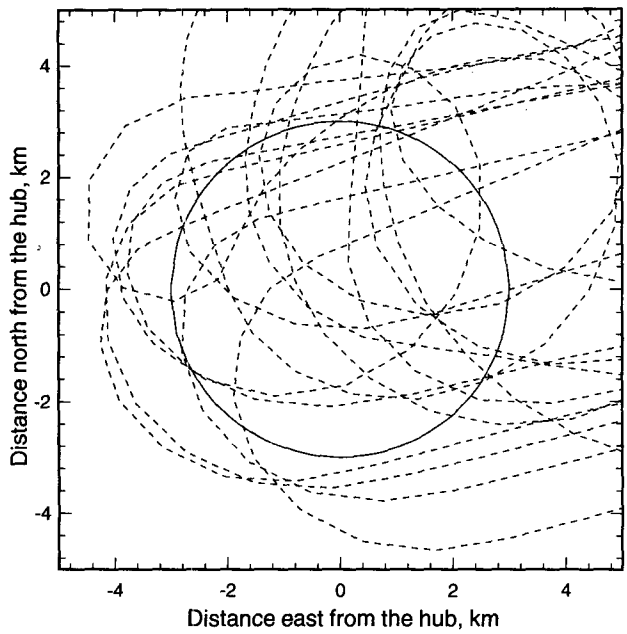

FIG. 10. (a) King Air flight tracks during the period from 1830 to 2130 UTC November 26 1991, hub location is (0, 0). (b) King Air flight tracks (dashed lines) above the hub. The solid line represents a circle with a 3-km radius with a center at the hub.

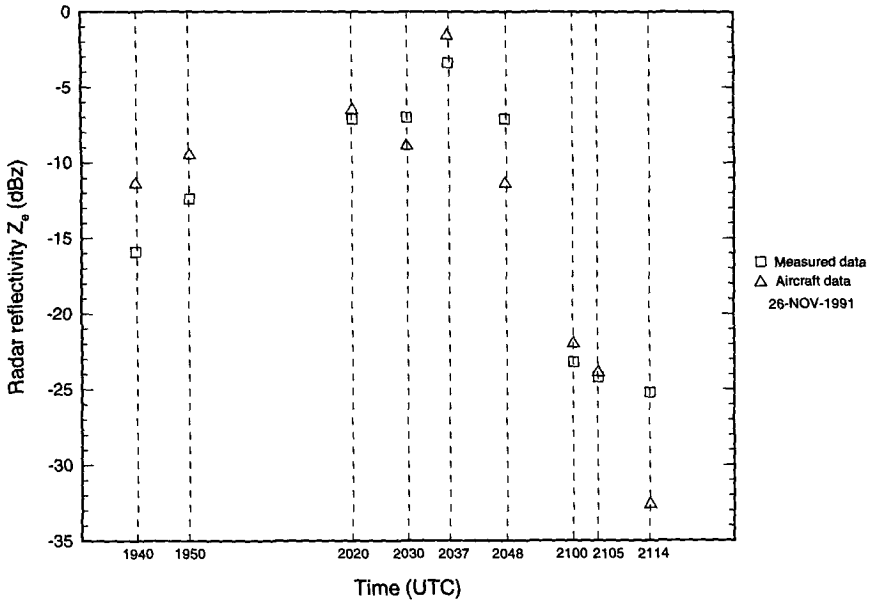

FIG. 11. Comparison of radar reflectivity (Z_e) values measured by the radar with that calculated from in situ 2D probes during the times of aircraft passes approximately above the hub.

2037, 2048, 2100, 2105, and 2114 UTC, respectively. Average altitudes of these passes were 8.54, 8.54, 7.62, 7.15, 7.10, 6.16, 6.25, 7.37, and 6.10 km, respectively. These nine passes provided nine points for comparison of the particle sizes retrieved from RRT method and those measured onboard the aircraft. Note that crossing of the 3-km radius circle still does not guarantee that the aircraft and remote measurements were made in the same cloud volume. The hope is, however, that the aircraft and the ground-based instruments were sampling nearly the same cloud volumes.

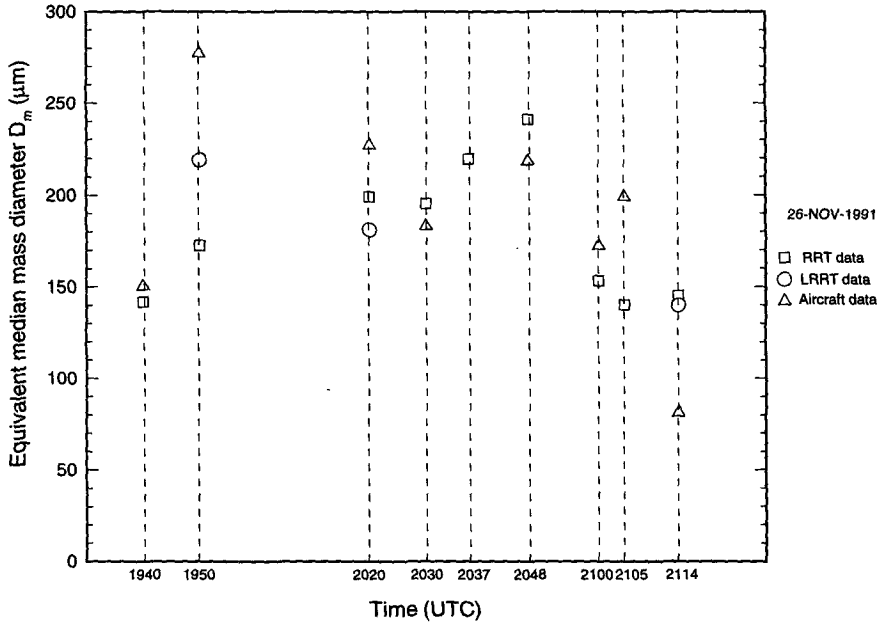

FIG. 12. Comparison of particle equivalent median diameter (D_m) retrieved by the radar–radiometer technique (RRT), lidar–radar–radiometer technique (LRRT), and calculated from in situ 2D probes during the times of aircraft passes nearly above the hub.

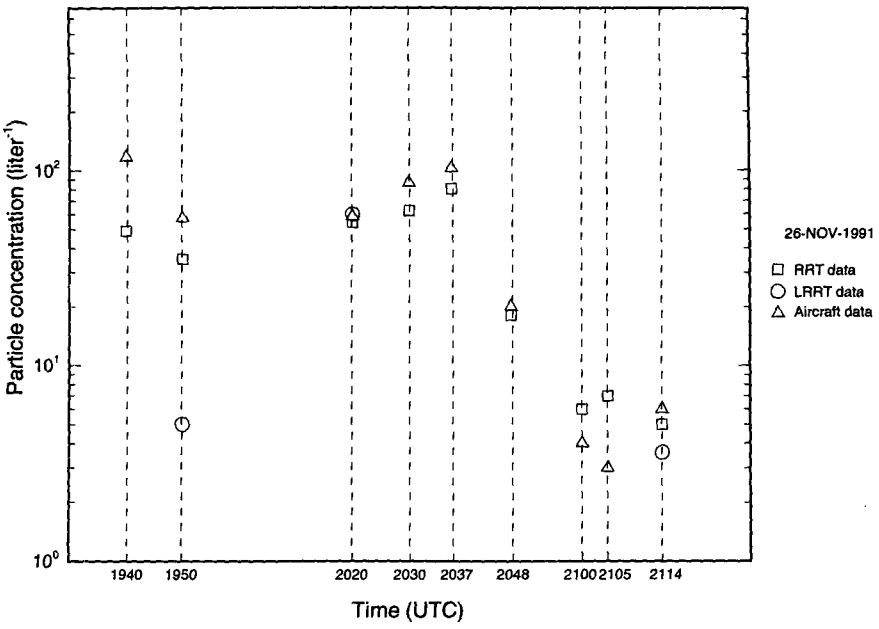

FIG. 13. Comparison of particle concentrations, C, retrieved by the radar–radiometer technique (RRT) with that calculated from in situ 2D probes during the times of aircraft passes approximately above the hub.

Except for one aircraft pass (2114 UTC), CO_2 lidar signals were completely attenuated inside the cloud during the times of comparison. However, at 1950 and 2020 UTC lidar signals penetrated only to about 2 km above the cloud bottom. During these times (1950 and 2020 UTC), the aircraft sampled the lower part of the cloud where lidar signals had not yet been completely attenuated and microphysical information from the LRRT method was available after accounting for the attenuation. Thus, three points were available for comparison of results obtained with LRRT method and in situ data.

Visual analysis of particle habits from 2D images showed that column type and bullet-rosettes were the dominant shapes in the particle samples. The aspect ratios of complex sampled particles were about 2. As mentioned earlier, this analysis was the primary reason for assuming prolate-shaped particles with aspect ratio $p = 2$ when performing the retrieval of microphysical parameters using the RRT method.

Figure 11 shows a comparison of radar reflectivity values, Z_e, measured by the radar with values calculated from the 2D probes. One can see that differences between measured and calculated reflectivities did not exceed 5 dB (except for 2114 UTC). When making comparisons at specific times, all aircraft data samples along the track for each pass of the 3-km radius circle were averaged.

Figure 12 shows a comparison of cloud particle sizes retrieved by the RRT and LRRT methods with those estimated from the microphysical sampling aboard the aircraft. The comparison is given in terms of equivalent median diameter (i.e., median mass diameter of the equal-volume sphere) D_m, assuming prolate-shape particles with the aspect ratio $p = 2$, in the case of the RRT method data. For the aircraft data 2D size values were converted to D_m values using Eq. (A7) from the appendix. For the LRRT data particle size in Fig. 12 is given in actual diameter because, as mentioned earlier, the current version of the LRRT method assumes a spherical particle shape.

The relative deviations of D_m, estimated using the aircraft sampling, from those obtained with the remote sensing methods were calculated using Eqs. (5) and (6). The calculation yielded $d_1 \approx 7\%$ and $d_2 \approx 30\%$ for the RRT method when the summation was done for all nine comparisons. In the case of the LRRT method the corresponding deviations, calculated only for three points of comparison, yielded $d_1 \approx 4\%$ and $d_2 \approx 35\%$, respectively. One can see that the general agreement between sizes retrieved from ground-based measurements and those calculated from the 2D probes is quite good, given the uncertainties of the different approaches.

The particle size information derived from the remote measurements and measured radar reflectivity values can also be used to estimate particle concentrations. Figure 13 compares retrieved values of concentration, C, retrieved with the RRT method with those calculated from King Air 2D probes for the times when aircraft samples were taken approximately above the hub.

Calculations of relative deviations of 2D probe concentrations from those retrieved with the RRT method C yielded $d_1 \approx 15\%$ and $d_2 \approx 60\%$. The general agreement shown in Fig. 13 could be considered satisfactory given the high variability of particle concentration in cirrus clouds. Note that, compared to particle sizes, retrieved values of particle concentrations are much more sensitive to the assumption about the shape of size distribution.

5. Conclusions

The FIRE II data of November 26 1991 provided a good opportunity to test different remote sensing methods and to compare cirrus cloud microphysical parameters retrieved by these methods with in situ data obtained from 2D particle probes aboard the aircraft. The retrieval performed with the radar–radiometer technique (RRT) (Matrosov et al. 1994) for the 3-hour period from 1830 to 2130 UTC, assuming prolate-shaped particles, showed a general gradual increase of characteristic particle sizes as the cloud developed/advected during the time of observation. Particle sizes were generally increasing toward the cloud base.

The sensitivity analysis of particle size retrieval by the RRT method showed that the particle bulk density–size relationship is the most important a priori assumption. The increase in the proportionality coefficient in this relationship (2) by 35% causes about 14% variation in retrieved particle sizes.

Variation in the assumed particle size distribution from the first-order Gamma function to the zero-order gamma function results in changes of the retrieved equivalent median diameter D_m of only a few percent. Changes in the assumed particle shapes from $p = 2$ to spheres (assuming constant bulk density) cause only a few percent variation in D_m. Such small size changes due to the assumed shape can be explained by the fact that accounting for nonsphericity in the extinction (IR) and reflectivity (radar) parts of the inverse problem (Matrosov et al. 1994) produces errors of opposite sign. These errors partially cancel out when retrieving values of D_m. However, the RRT retrieval scheme suggests changes in particle bulk density through the changes in shape [see (2)]. This results in about a 20% change in retrieved D_m due to variation of p from 2 to 1.

An inadequate removal of mean air motion of order 7 cm s^{-1} when estimating particle fall velocities can result in errors in the retrieved size of about 9%. This constant height-independent shift in estimated particle fall velocities representing a possible updraft does not change retrieved sizes significantly, because real measurements of cloud optical thickness are used to normalize fall velocity–size relationships.

Comparisons of the particle sizes retrieved by the radar–radiometer technique (RRT) and the lidar–radar–radiometer technique (LRRT) (Intrieri et al. 1993) were available for only two periods, either because of the attenuation of lidar signals in the upper parts of the cloud or sensors performing scanning modes. The relative standard deviation (d_2) of particle sizes D_m obtained with these two remote sensing approaches, under identical assumptions about particle shape and density (solid ice spheres), were about 15%–20%.

The relative standard deviation of particle size retrieved with both the RRT and LRRT methods, from those measured using 2D particle probes aboard the King Air aircraft during the passes above the hub, was about 30%–35%. The comparisons were made during nine aircraft passes above the hub in the case of the RRT method and during three such passes in the case of the LRRT method.

For the nine aircraft passes, comparison of particle concentrations obtained with the RRT method with those from the aircraft 2D probes yielded about 60% for the relative standard deviation of in situ results from the retrieved data.

Acknowledgments. The authors would like to thank Yong Han for performing FASCODE calculations, Marcia Politovich for providing aircraft track information, and R. A. Kropfli and B. E. Martner for valuable discussions. B. W. Bartram and K. A. Clark were responsible for the performance of the ETL K_a-band radar. This work was funded, in part, through a grant from the Environmental Science Division of the U.S. Department of Energy and by the NOAA Climate and Global Change Program Office.

APPENDIX

Relationship Between 2D Particle Size and Diameter of Equal-Volume Spheres

In this section we suggest a relationship between experimentally measured and theoretically modeled particle sizes. The experimental particle size from aircraft probes L is the projection of this particle either along ($L_\parallel$) or perpendicular ($L_\perp$) to the axis of the 2D probe, which ever is larger:

$$L = \max(L_\parallel, L_\perp). \tag{A1}$$

Let the axis of the 2D probe be the OY axis and the perpendicular axis be the OZ axis of the Cartesian coordinate system. A blocky spheroidal particle with dimensions L_1 and L_2 (L_1 and L_2 are measured along the particle symmetry axis and perpendicular to it, respectively) is assumed to be randomly oriented with respect to this system. Using a simple geometrical approach, one can get approximations for the particle projections $L_\parallel$ and $L_\perp$

$$L_\parallel^2 = (L_2^2 \cos^2\psi + L_1^2 \sin^2\psi) \sin^2\alpha + L_2^2 \cos^2\alpha, \tag{A2}$$

$$L_\perp^2 = (L_2^2 \cos^2\psi + L_1^2 \sin^2\psi) \cos^2\alpha + L_2^2 \sin^2\alpha, \tag{A3}$$

where ψ and α are the angles between the particle symmetry axis and the negative direction of the OX axis, and between the projection of the particle symmetry axis on the ZOY plane and the OZ axis. Angles ψ and α can be expressed in terms of the polar coordinate angles θ and ϕ of the particle symmetry axis (Holt 1984):

$$\cos\alpha \cdot \sin\psi = \cos\theta \quad \text{(A4)}$$

$$\sin\alpha \cdot \sin\psi = \sin\theta \cdot \sin\phi \quad \text{(A5)}$$

$$\cos\psi = -\sin\theta \cdot \cos\phi. \quad \text{(A6)}$$

The coefficient r_L is defined as the ratio of the 2D particle size L to the diameter of the equal volume sphere D:

$$r_L = L/D. \quad \text{(A7)}$$

Relations between D and L_1 and L_2 for prolate and oblate spheroids are given by

$$L_1 = Db^{-2/3} \quad \text{(A8)}$$

$$L_2 = Db^{1/3} \quad \text{(A9)}$$

$$L_1 = Db^{2/3} \quad \text{(A10)}$$

$$L_2 = Db^{-1/3}, \quad \text{(A11)}$$

where Eqs. (A8) and (A9) are for prolate spheroids and (A10) and (A11) are for oblate spheroids and b is the particle minor to major ratio ($b = 1/p$).

The mean ratio r_L can be calculated from the integral

$$r_L = \frac{1}{4\pi D}\int_0^{2\pi}\int_0^{\pi} \max(L_\parallel, L_\perp)\sin\theta d\theta d\phi. \quad \text{(A12)}$$

REFERENCES

Atlas, D. M., M. Kerker, and W. Hitschfeld, 1953: Scattering and attenuation by non-spherical atmospheric particles. *J. Atmos. Terr. Phys.*, **3**, 108–119.

Chylek, P., and G. Videen, 1994: Longwave radiative properties of polydispersed hexagonal ice crystals. *J. Atmos. Sci.*, **51**, 175–190.

Clough, S. A., R. D. Worsham, W. L. Smith, H. E. Revercopmb, R. O. Knuteson, H. W. Woolf, G. P. Anderson, M. L. Hoke, and F. X. Kneizys, 1988: Validation of FASCODE calculations with HIS spectral radiance measurements. *Proc. Int. Radiation Symp.*, Lille, France, A. Deepak, 376–379.

Dungey, C. E., and C. F. Bohren, 1993: Backscattering by nonspherical hydrometeors as calculated by the coupled-dipole method: An application in radar meteorology. *J. Atmos. Oceanic Technol.*, **10**, 526–532.

Ebert, E. E., and J. A. Curry, 1992: A parameterization of ice cloud optical properties for climate models. *J. Geophys. Res.*, **97**, 3831–3836.

Heymsfield, A. J., 1975: Cirrus uncinus generating cells and the evolution of cirriform clouds. Part I: Aircraft observations of the growth of the ice phase. *J. Atmos. Sci.*, **32**, 799–808.

——, K. M. Miller, and J. D. Spinhirne, 1990: The 27–28 October 1986 FIRE IFO cirrus case study: Cloud microstructure. *Mon. Wea. Rev.*, **118**, 2313–2328.

Holt, A. R., 1984: Some factors affecting the remote sensing of rain by polarization diversity radar in the 3- to 35-GHz frequency range. *Radio Sci.*, **19**, 1399–1421.

Illingworth, A. J., 1994: Spaceborne cloud radar: Sampling and retrievals. Report of the GEWEX topical workshop, World Meteorological Organization, International GEWEX Program Office, Publ. series No. 10, B48–B53.

Intrieri, J. M., G. L. Stephens, W. L. Eberhard, and T. Uttal, 1993: A method for determining cirrus cloud particle sizes using lidar and radar backscatter technique. *J. Appl. Meteor.*, **32**, 1074–1082.

——, T. Uttal, W. L. Eberhard, J. B. Snider, Y. Han, J. A. Shaw, B. W. Orr, and S. Y. Matrosov, 1995: Multiwavelength observations of a developing cloud system: The FIRE II 26 November 1991 case study. *J. Atmos. Sci.*, **52**, 4079–4093.

Kosarev, A. L., and I. P. Mazin, 1989: Empirical model of physical structure of the upper level clouds of the middle latitudes. *Radiation Properties of Cirrus Clouds*, Nauka, 29–52.

Lin, X., 1993: Cloud droplet/particle sizes obtained from emitted radiances. *Proc. SPIE*, **1934**, 354–360.

Magono, C., and C. W. Lee, 1966: Meteorological classification of natural snow crystals. *J. Fac. Sci. Hokkaido Univ. Ser.* **7**(2), No. 4,321–335.

Matrosov, S. Y., 1993: Possibilities of cirrus particle sizing from dual-frequency radar measurements. *J. Geophys. Res.*, **98**, 20 675–20 683.

——, T. Uttal, J. B. Snider, and R. A. Kropfli, 1992: Estimation of ice cloud parameters from ground-based infrared radiometer and radar measurements. *J. Geophys. Res.*, **97**, 11 567–11 574.

——, B. W. Orr, R. A. Kropfli, and J. B. Snider, 1994: Retrieval of vertical profiles of cirrus cloud microphysical parameters from Doppler radar and infrared radiometer measurements. *J. Appl. Meteor.*, **33**, 617–626.

Minnis, P., K.-N. Liou, and Y. Takano, 1993: Inference of cirrus cloud properties using satellite visible and infrared radiances. Part I: Parameterization of radiance fields. *J. Atmos. Sci.*, **50**, 1279–1304.

Mitchell, D. L., J. E. Kristjansson, and M. J. Newman, 1994: Sensitivity of cirrus cloud radiative properties to ice crystal size and shape in GCM simulations. Preprints, *Eighth Conf. on Atmospheric Radiation*, Nashville, TN, Amer. Meteor. Soc., 552–554.

Ou, S. C., K. N. Liou, and N. X. Rao, 1994: Remote sounding of cirrus cloud optical depth and ice crystal size using AVNRR data. Preprints, *Eighth Conf. on Atmospheric Radiation*, Nashville, TN, Amer. Meteor. Soc., 394–395.

Parol, F., J. C. Buriez, G. Brogniez, and Fouquart, 1991: Information content of AVHRR channels 4 and 5 with respect to the effective radius of cirrus cloud particles. *J. Appl. Meteor.*, **30**, 973–984.

Platt, C. M. R., and A. C. Dilley, 1979: Remote sounding of high clouds: Emissivity of cirrostratus. *J. Appl. Meteor.*, **18**, 1144–1150.

Pruppacher, H. R., and J. D. Klett, 1978: *Microphysics of Clouds and Precipitation*. D. Reidal, 714 pp.

Schneider, T. L., and G. L. Stephens, 1994: Backscattering by nonspherical ice particles at millimeter wavelengths. Preprints, *Eighth Conf. on Atmospheric Radiation*, Nashville, TN, Amer. Meteor. Soc., 310–312.

Stamnes, K., S. C. Tsay, W. Wiscombe, and K. Jayaweera, 1988: Numerically stable algorithm for discrete-ordinate-method radiative transfer in multiple scattering and emitting layered media. *Appl. Optics*, **27**, 2502–2509.

Takano, Y., K. N. Liou, and P. Minnis, 1992: The effect of small ice crystals on cirrus radiative properties. *J. Atmos. Sci.*, **49**, 1487–1493.

Young, D. F., S. Mayor, P. Minnis, J. M. Intrieri, S. Y. Matrosov, and J. B. Snider, 1994: Comparisons of satellite and surface-based remote sensing of cloud microphysical properties during FIRE cirrus phase II. Preprints, *Eighth Conf. on Atmospheric Radiation*, Nashville, TN, Amer. Meteor. Soc., 231–233.